The Proposed Interferometric-Type Laser-Driven Particle Accelerators

Y.C. Huang[1], Y.W. Lee[1], T. Plettner[2], and R.L.Byer[2]

[1]*Department of Atomic Science*
National Tsinghua University, Hsinchu, Taiwan 30043

[2]*Department of Applied Physics*
Stanford University, Stanford, CA 94305-4085

Abstract In a crossed-laser-beam accelerator, two properly phased laser beams, forming an interferometric configuration, may provide an adequate particle acceleration field over a phase matching distance. The two laser beams can be obtained by dividing a full, Gaussian laser beam equally in amplitude or in wavefront. We show in this paper that a wavefront-splitting laser-driven accelerator is relatively simple to set up and provides an acceleration gain comparable to that of an amplitude-splitting accelerator under the same laser damage fluence. We also present the noise characteristics measured from various interferometers, which may be useful for implementing interferometric-type accelerators.

INTRODUCTION

In the past several decades, conventional RF accelerators have successfully generated GeV electrons with an average acceleration gradient of a few tens MeV per meter. The average gradient is limited by field-induced structure damage. The damage threshold is determined by the driving frequency, the pulse duration, and the structure material. To increase the acceleration gradient, recent research interests have moved toward higher operation frequencies including those in the millimeter-wavelength and optical regimes[1, 2]. A high-frequency accelerator has the additional advantage of producing short electron bunches, which might be important in the future for generating coherent UV or x-ray[3].

To develop optical-frequency accelerators, efforts at Stanford University are being made in the experimental demonstration of crossed-laser-beam electron linear acceleration between two dielectric boundaries[4]. Although plasma-based laser-driven accelerators have demonstrated a ~100 GeV/m peak gradient over a submillimeter distance[5], theoretical studies indicate that a dielectric-based, laser-driven accelerator might achieve a ~1 GeV/m average gradient over a much longer distance[6].

According to the Lawson-Woodward theorem[7], first-order energy transfer from a photon to an electron can not occur in a vacuum. To obtain electron linear acceleration

CP472, *Advanced Accelerator Concepts: Eighth Workshop*,
edited by W. Lawson, C. Bellamy, and D. Brosius

from a laser field, Pantell *et al.*[8,9] proposed to cross an electron beam with a linearly polarized laser beam at an angle and limit the interaction length to a phase slip less than π. To avoid any transverse force acting on the electron, a symmetric crossed-laser-beam acceleration scheme was proposed and analyzed by several authors[10,11,12]. The two laser beams in the proposed configurations are phased such that transverse-field components cancel and longitudinal-field components add along the electron axis. Figure 1 illustrates the symmetric, crossed-laser-beam accelerator configuration. The primed coordinate system defines the rotated laser beam axis, and the unprimed one includes the electron axis. Huang and Byer[13] extended the idea of the proposed accelerator to a configuration whose structure dimensions and the laser fields are constant in y. This novel design allows for the acceleration of more charge, reduced thermal loading, and decreased wake field generation.

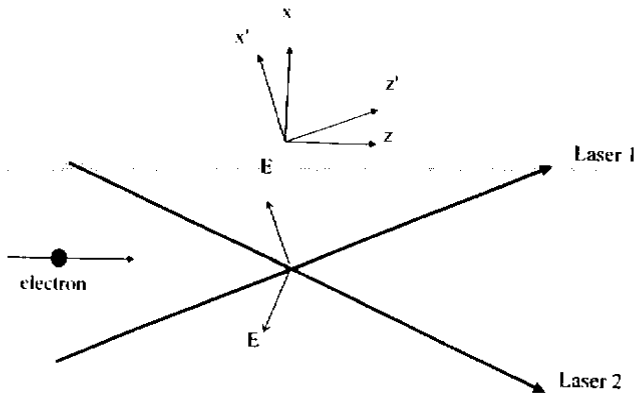

FIGURE 1. The proposed crossed-laser-beam accelerator configuration. Two linearly polarized laser pulses are crossed at an angle with respect to the electron trajectory. The two laser beams are phased such that their longitudinal electric fields add and their transverse electric fields cancel on the electron axis. The primed coordinate system defines the rotated laser beam axis, and the unprimed one includes the electron axis. The laser fields are constant in y.

Since the two laser beams form interference fringes in the transverse direction, in this paper we term the proposed structures interferometric-type accelerators. The distribution of the interference fringes indicates a proper longitudinal field for particle acceleration, as will be discussed.

ACCELERATION FIELDS

In a linear accelerator, there ought to be a longitudinal electric field component in the acceleration direction or the z-direction defined in this paper. An observation from the divergent-free electric field vector $\nabla \cdot \vec{E} = 0$ indicates that the

longitudinal field component E_z is coupled to the transverse electric field E_x through the approximation[14]

$$\tilde{E}_z \approx \frac{j}{k}\frac{\partial \tilde{E}_x}{\partial x}, \tag{1}$$

where $k \equiv \frac{2\pi}{\lambda}$ is the wave number, $j \equiv \sqrt{-1}$ is the imaginary unit, and the tilde designates phasor notations. In Eq. (1), the approximation comes from the assumption of a slowly varying laser field envelope along z. In an ideal accelerator it is desirable to have no transverse field on the electron axis or $E_x(x=0)=0$. To obtain a net E_z along z, it is evident from (1) and the condition $E_x(x=0)=0$ that E_x is an odd function in x. For example, the superposition of two crossed, equal-amplitude plane waves gives the following two electric field components:

$$E_x = 2E_0\cos\theta\cdot\cos(kx\sin\theta+\varphi/2)\cdot\cos(\omega t - kz\cos\theta+\varphi/2), \tag{2}$$
$$E_z = -2E_0\sin\theta\cdot\sin(kx\sin\theta+\varphi/2)\cdot\sin(\omega t - kz\cos\theta+\varphi/2), \tag{3}$$

where E_0 is the field amplitude of each plane wave, θ is the crossing angle relative to the electron axis, φ is an arbitrary phase difference between the two waves, and ω is the angular frequency. To maximize the z-component field on the electron axis φ is set to be π. Thus Eqs. (2, 3) become

$$E_x = 2E_0\cos\theta\cdot\sin(kx\sin\theta)\cdot\sin(\omega t - kz\cos\theta), \tag{4}$$
$$E_z = -2E_0\sin\theta\cdot\cos(kx\sin\theta)\cdot\cos(\omega t - kz\cos\theta), \tag{5}$$

which clearly show that E_x is an odd function in x. In this crossed-laser-beam configuration, the laser power propagates primarily in the z-direction and thus the interference intensity along x is mostly due to E_x, given by

$$I(x) = 2E_0^2\cos^2\theta\cdot\cos^2(kx\sin\theta+\varphi/2). \tag{6}$$

For $\varphi=\pi$, a dark interference fringe appears at $x=0$ and therefore it indicates a z-component electric field for particle acceleration.

There are two types of interferometers, amplitude-splitting interferometers and wavefront-splitting interferometers[15]. Therefore the proposed accelerator configurations can be divided into two categories: amplitude-splitting accelerators and wavefront-splitting accelerators.

AMPLITUDE-SPLITTING ACCELERATORS

Figure 2.a illustrates the proposed amplitude-splitting accelerator configuration

where a full-Gaussian laser beam is split equally in amplitude to form two crossed Gaussian laser beams inside the accelerator cell. An external phase controller sets the relative phase $\varphi = \pi$ between the two laser beams. Figure 2.b shows the interference fringes in x formed by two cylindrical Gaussian laser beams at the focal point. The dark fringe appearing at $x = 0$ is a signature of the longitudinal field for particle acceleration, as shown in the last section. Unlike the constant-amplitude fringes in Eq. (6) from two plane waves, Fig. 2.b shows an attenuating envelope in $|x|$ due to the Gaussian laser field distribution. In the plot we choose a laser crossing angle of 50 mrad, a laser waist size of 25 μm, and a laser wavelength of 1 μm.

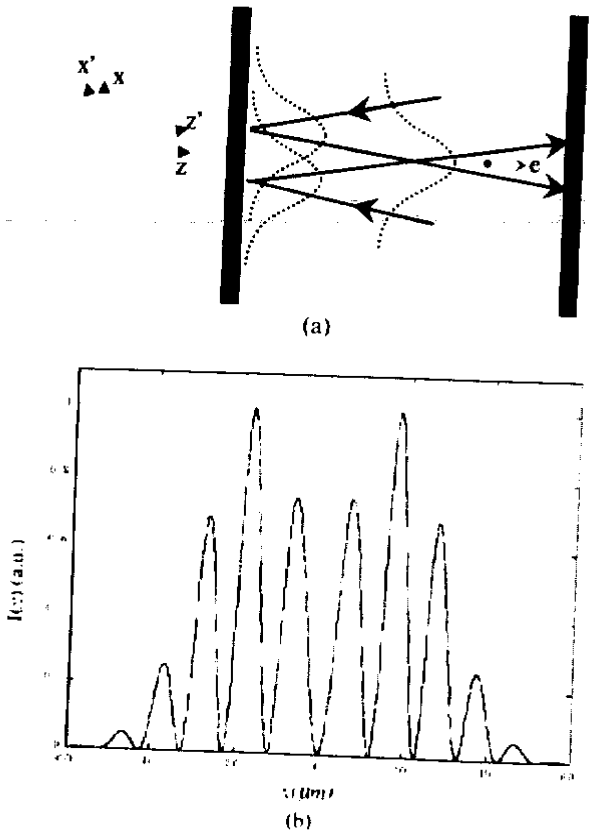

FIGURE 2. (a) The proposed amplitude-splitting accelerator configuration where a full-Gaussian laser beam is split equally in amplitude to form crossed laser beams inside the accelerator stage. An external optical phase controller sets the relative phase between the two laser beams. (b) The interference fringes in x formed by two cylindrical Gaussian laser beams at the focal point. The dark fringe appearing at $x = 0$ is a signature of the longitudinal electric field for particle acceleration.

The electron energy gain of the proposed accelerator structure in Fig. 2.a can be calculated by integrating the z-component electric field of two superimposed, cylindrical, Gaussian laser beams. Structure damage by intense laser fields limits the acceleration gradient. At the dielectric damage fluence 2J/cm^2 for ~100 fsec laser pulses[16], a 280 keV electron energy gain[13] is predicted for an interaction length of 340 μm.

WAVEFRONT-SPLITTING ACCELERATORS

Figure 3 illustrates the proposed wavefront-splitting accelerator configuration where a full-Gaussian laser beam is split equally in wavefront to form two crossed, half-Gaussian beams at the coupling point. The $\phi = \pi$ phase shift in Fig. 3 is set by a phase step at the laser coupling point. The half-Gaussian laser fields in Fig. 3 can be numerically synthesized by superimposing many plane waves propagating at different angles and amplitudes[17]. Specifically an arbitrary vector-field component $\widetilde{E}_x(x,z)$ in x can be expressed by

$$\widetilde{E}_x(x,z) = \int_{-\pi/2}^{\pi/2} a(\phi)\cos\phi \times \exp(-jkx\sin\phi - jkz\cos\phi)\,d\phi \tag{7}$$

and the corresponding $\widetilde{E}_z(x,z)$ of the wave is

$$\widetilde{E}_z(x,z) = \int_{-\pi/2}^{\pi/2} a(\phi)\sin\phi \times \exp(-jkx\sin\phi - jkz\cos\phi)\,d\phi\,. \tag{8}$$

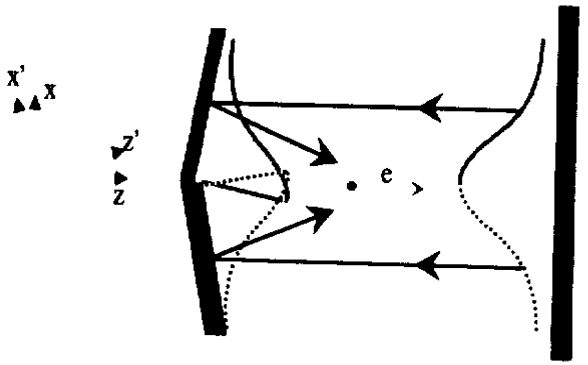

FIGURE 3. The proposed wavefront-splitting accelerator configuration where a full-Gaussian laser beam is split equally in wavefront to form two half-Gaussian beams at the coupling point. The $\phi = \pi$ phase shift between the two beams is set by a phase step on the corner reflector.

As long as the angular spectrum $a(\phi)$ is known, the vector fields $\tilde{E}_x(x,z)$ and $\tilde{E}_z(x,z)$ everywhere in space can be determined from Eqs. (7, 8). The angular spectrum $a(\phi)$ is evaluated numerically from Eq. (7) by knowing the boundary field $\tilde{E}_x$ at the coupling point, which is essentially the transverse field sum of an angle-tilted Gaussian laser beam.

Integrating the thus-obtained z-component electric field gives the electron energy gain. Figure 4 illustrates the electron energy gain along a 340 μm interaction length for the amplitude-splitting accelerator in Fig. 2.a and the wavefront-splitting accelerator in Fig. 3. In our calculation the laser crossing angle is 50 mrad and the laser wavelength is 1 μm. We have assumed relativistic electrons, that is $\gamma >> 1/\theta$, where γ is the electron energy in units of the electron rest-mass energy and θ is the laser-electron crossing angle. Before split in wavefront, the full Gaussian beam in Fig. 3 has a waist size of 50 μm, twice that in Fig. 2.a. Thus the total laser power for acceleration and the laser damage intensity on the dielectric surface remain the same for both accelerator structures. The electron entrance phase for each case is adjusted to obtain the highest electron energy gain. For this particular set of parameters, the energy gain of the wavefront-splitting accelerator is about 15% lower due to the phase slip caused by large-angle plane-wave components at the coupling point. Numerical calculation shows that the single-stage energy gain of a wavefront-splitting accelerator need be only 10% lower than the amplitude-splitting interferometric accelerator when the laser crossing angle in Fig. 3 is reduced to 40 mrad.

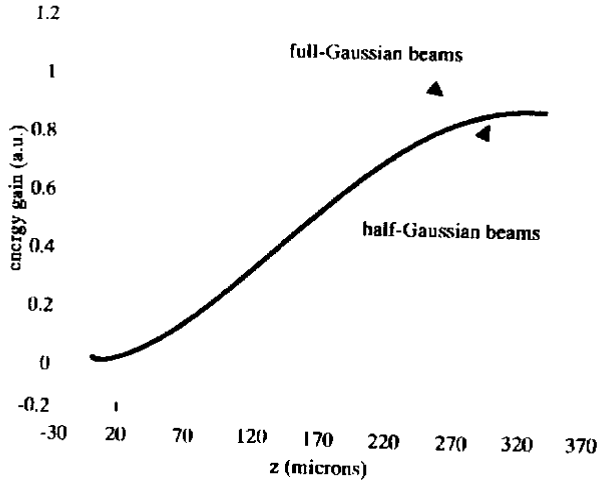

FIGURE 4. The electron energy gain along a 340 μm interaction length for the proposed amplitude-splitting accelerator and the wavefront-splitting accelerator. Both accelerators have the same laser damage intensity on the dielectric surfaces and the same laser power inside the accelerators. The laser crossing angle is 50 mrad and the laser wavelength is 1 μm. For this particular case, the electron energy gain of the wavefront splitting accelerator is lower by 15%.

NOISE CHARACTERISTICS

Scaled to optical wavelengths, a laser-driven accelerator structure size is much smaller than a RF accelerator. The micron wavelength, together with the small structure size, imposes stringent requirements on optical phase control. In order to increase the phase coherence length and thus the accelerator size, the laser crossing angle in the proposed accelerators is typically of a few milliradians and the accelerator length is of a few hundred microns for a 1-μm laser wavelength[13]. Because of the small crossing angle and the large laser field $E_0 \approx 10$ GV/m, slight asymmetry in laser coupling or a small phase mismatch in ϕ could result in a large transverse field on the electron axis, as Eq. (2) indicates. Furthermore, recombining two sub-picosecond laser pulses within a small optical phase angle appears to be nontrivial. For example, overlapping the optical phase of two laser pulses within a one-degree angle requires a temporal precision of 10 atoseconds for a 1-μm laser wavelength. In view of the above, we argue that the proposed wavefront-splitting structure in Fig. 3 offers potential advantages over the amplitude splitting structure in Fig. 2.a. The reasons are:

1. In Fig. 3, the π relative phase between the two laser beams is set by a dielectric phase step on the corner reflector. The thickness of the dielectric step can be fabricated precisely by using optical coating or lithographic techniques.
2. In Fig. 3, since the source laser pulse is divided in wavefront at the accelerator coupling point, recombining the two wavefront-splitting laser pulses can be achieved with a great accuracy in time or in optical phase. The tilting angle between the two coupling mirrors determines the laser-crossing angle.

In addition, the wavefront-splitting structure is apparently immune from background acoustic noise. An acoustic wave in a solid typically has a wavelength of a few centimeters, which is much longer than a laser-driven particle accelerator structure. The accelerator stage occupies a very small phase of the acoustic wave. As a result, if the laser pulse splitting point is within the accelerator, as is the case for a wavefront-splitting accelerator, the relative optical phase of the two laser pulses remains fixed regardless of background vibration. An amplitude-splitting interferometer typically has more discrete elements, and requires a better technique in micro-fabrication or a noise-proof interferometer design.

As shown in Eq. (6), the stability of the interference fringes in x manifests the noise characteristics of the proposed interferometric-type accelerators. In our noise measurements, the amplitude-splitting interferometer, mimicking the proposed structure in Fig. 2.a, is a Mach Zehnder interferometer and a Sagnac interferometer; whereas the wavefront-splitting interferometer, mimicking the proposed structure in Fig. 3, is a Fresnel two-mirror interferometer.

Figure 5.a illustrates the noise measurement setup for a Mach Zehnder interferometer and a Fresnel two-mirror interferometer; Fig. 5.b illustrates that for a Sagnac interferometer and a Fresnel two-mirror interferometer. A 3.5 mW, 670 nm-wavelength diode laser (LD) drives the two interferometers via a 50% beam splitter (BS1). Thus any noise from the diode laser and BS1 is common to both

interferometers. Each of the two Fresnel mirrors is a 5 mm × 5 mm square silver reflector. The Mach Zehnder interferometer or the Sagnac interferometer occupies a 4 cm × 4 cm area, which is the smallest that we could build by using one-inch diameter optics (M1, M2, BS2, BS3). We adjusted the interferometers until we saw clear interference fringes on a screen. A 1 cm diameter PIN diode detector, covering the whole interference pattern, takes the laser signal into a Stanford Research SR780 spectrum analyzer for noise measurements.

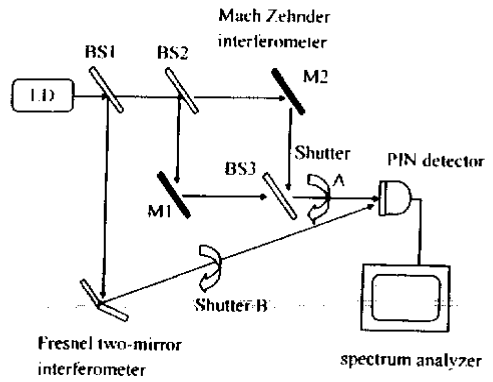

(a)

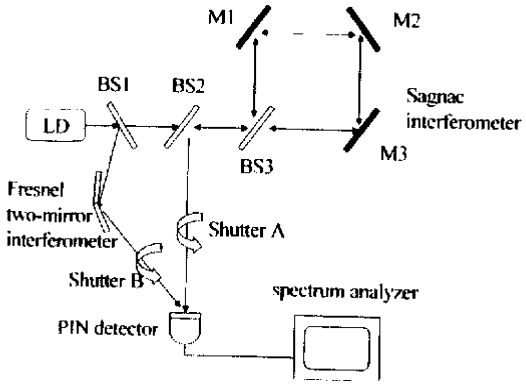

(b)

FIGURE 5. Noise measurement setups. (a) Mach Zehnder interferometer and Fresnel two-mirror interferometer. (b) Sagnac interferometer and Mach Zehnder interferometer.

We measured the root-mean-square noise spectra for the following three situations:

1. Both Shutters A and B are closed. This measurement gives the electronic noise floor.
2. Shutter A is closed and Shutter B is opened. This measurement gives the noise spectrum of the Fresnel two-mirror interferometer.
3. Shutter B is closed and Shutter A is opened. This measurement gives the noise spectrum of the Mach Zehnder interferometer or the Sagnac interferometer.

Our measurements show no difference between the electronic noise floor and the noise spectrum of the Fresnel two-mirror interferometer. In fact, we visually noticed steady interference fringes from the Fresnel two-mirror interferometer, whereas blinking fringes from the Mach Zehnder interferometer. A Sagnac interferometer is a common-path interferometer, which rejects any noise symmetric to the two optical paths. In our experiments, the phase stability of a Sagnac interferometer is obviously better than a Mach Zehnder interferometer, but slightly worse than a Fresnel two-mirror interferometer. Figure 6.a shows the noise spectra of the Fresnel two-mirror interferometer and the Mach Zehnder interferometer between 10 Hz and 0.8 kHz with a 2 Hz resolution. Although the laser power of the Mach Zehnder interferometer is a factor of two lower due to the third beam splitter BS3, the noise amplitude of the 4 cm × 4 cm Mach Zehnder interferometer is apparently several orders of magnitude higher on the low frequency side. Figure 6.b shows the noise spectra of the Fresnel two-mirror interferometer and the Sagnac interferometer. The Sagnac interferometer is much less sensitive to acoustic noise when compared to the Mach Zehnder interferometer, but still slightly worse than the Fresnel two-mirror interferometer. Without miniaturizing the three interferometers, this preliminary result indicates

1. A wavefront-splitting accelerator is simple to set up and insensitive to background acoustic noise.
2. A Sagnac interferometer is less sensitive to noise and is a better choice for an amplitude-splitting accelerator.

CONCLUSIONS

The particle acceleration field of an interferometric-type laser-driven accelerator can be obtained from an amplitude-splitting interferometric configuration or a wavefront-splitting configuration. We have showed numerically that a wavefront-splitting accelerator configuration gives a single-stage electron energy gain comparable to that of an amplitude-splitting accelerator configuration under the same laser damage fluence. Our noise measurements qualitatively confirm that the optical phase stability of a wavefront-splitting interferometric laser-driven particle accelerator is more stable due to its monolithic construction. The proposed wavefront-splitting accelerator configuration essentially alleviates the cumbersome phase and timing control on femto-second laser pulses.

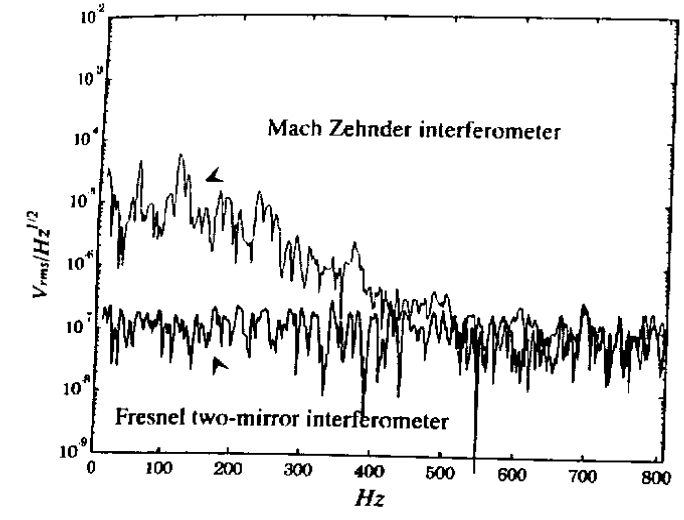

(a)

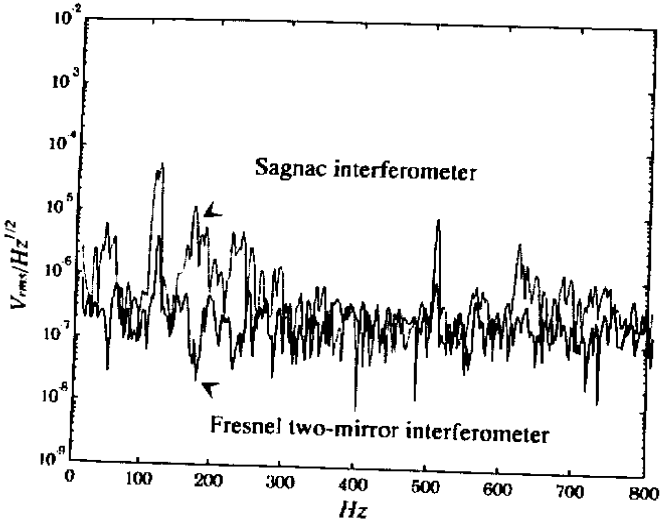

(b)

FIGURE 6. (a) The noise spectra of the Mach Zehnder interferometer and the Fresnel two-mirror interferometer. The noise amplitude of the Mach Zehnder interferometer is apparently much higher on the low-frequency side due to its discrete optical elements. (b) The noise spectrum of the Sagnac interferometer is not much worse than that of a Fresnel two-mirror interferometer.

ACKNOWLEDGMENTS

The work at National Tsinghua University, Taiwan, is supported by the National Science Council under the contract number NSC-87-2112-M-007-024, and that at Stanford University, U.S.A., is supported by the Department of Energy under the contract number DE-AC03-76SF00515.

REFERENCES

1. Chou, P.J., Bowden, G.B., Copeland, M.R., Menegat, A., and Siemann, R.H., SLAC-PUB-7498, May 1997.
2. Sprangle, P., Esarey, E., and Krall , J., *Phys. Plasmas* **3** (5), 2183-2188 (1996).
3. Huang , Y.C. and Byer, R.L., *Nucl. Inst. Meth.* A393, 11-37 (1997).
4. Huang, Y.C., et al. to be published in *Nucl. Inst. Meth. A* (1998).
5. Clayton, C. E., *et al.* and Nakajima, K. *et al.*, Proceedings of the Advanced Accelerator Concepts Workshop, Lake Tahoe, 1996 (AIP, NY, 1997), S. Chattopadhay editor.
6. Huang, Y.C. and Byer, R.L., *Appl. Phys. Lett.* **69** , 2175-2177 (1996).
7. Palmer, R.B., Lecture Notes in Physics 296, Frontiers of Particle Beams p. 607 (Springer, Berlin, 1988).
8. Edighoffer, J.A. and Pantell, R.H., *J. Appl. Phys.* **50** , p. 6120 (1979).
9. Pantell, R.H. and Piestrup, *Appl. Phys. Lett.* **32**, 1 (1978).
10. Haaland , C.M., *Opt. Comm.* **114**, p. 280 (1995).
11. Sprangle, P., Esarey, E., Krall, J., Ting, A., *Opt. Comms.* 124, p. 69 (1996).
12. Huang, Y.C., Zheng, D., Tulloch, W.M., and Byer, R.L., *Appl. Phys. Lett.* **68** , p. 753 (1996).
13. Huang, Y.C. and Byer, R.L., *Appl. Phys. Lett.* **69** , p. 2175 (1996).
14. Scully, M.O., *Appl. Phys.* B **51**,238-241 (1990).
15. Hecht , Optics, , 3rd edition, Addison Wesley Inc. 1998.
16. Stuart, B.C., Feit, M.D., Rubenchik, A.M., Shore, B.W., and Perry, M.D., *Phys. Rev. Lett.* v **74**, 2248-2251 (1995).
17. Edighoffer, J.A. and Pantell, R.H., *J. Appl. Phys.* **50** , 6120 (1979).